Continuous record of microparticle concentration and size distribution in the central Greenland NGRIP ice core during the last glacial period

Urs Ruth[1] and Dietmar Wagenbach
Institute of Environmental Physics, University of Heidelberg, Heidelberg, Germany

Jørgen P. Steffensen
Department of Geophysics, University of Copenhagen, Copenhagen, Denmark

Matthias Bigler
Department of Climate and Environmental Physics, University of Bern, Bern, Switzerland

Received 26 March 2002; revised 29 July 2002; accepted 12 September 2002; published 5 February 2003.

[1] A novel laser microparticle detector used in conjunction with continuous sample melting has provided a more than 1500 m long record of particle concentration and size distribution of the NGRIP ice core, covering continuously the period approximately from 9.5–100 kyr before present; measurements were at 1.65 m depth resolution, corresponding to approximately 35–200 yr. Particle concentration increased by a factor of 100 in the Last Glacial Maximum (LGM) compared to the Preboreal, and sharp variations of concentration occurred synchronously with rapid changes in the $\delta^{18}O$ temperature proxy. The lognormal mode μ of the volume distribution shows clear systematic variations with smaller modes during warmer climates and coarser modes during colder periods. We find $\mu \approx 1.7$ μm diameter during LGM and $\mu \approx 1.3$ μm during the Preboreal. On timescales below several 100 years μ and the particle concentration exhibit a certain degree of independence present especially during warm periods, when μ generally is more variable. Using highly simplifying considerations for atmospheric transport and deposition of particles we infer that (1) the observed changes of μ in the ice largely reflect changes in the size of airborne particles above the ice sheet and (2) changes of μ are indicative of changes in long range atmospheric transport time. From the observed size changes we estimate shorter transit times by roughly 25% during LGM compared to the Preboreal. The associated particle concentration increase from more efficient long range transport is estimated to less than one order of magnitude. *INDEX TERMS:* 0305 Atmospheric Composition and Structure: Aerosols and particles (0345, 4801); 0322 Atmospheric Composition and Structure: Constituent sources and sinks; 0368 Atmospheric Composition and Structure: Troposphere—constituent transport and chemistry; *KEYWORDS:* mineral dust, ice cores, size distribution, continuous flow analysis, atmospheric circulation, paleoclimate

Citation: Ruth, U., D. Wagenbach, J. P. Steffensen, and M. Bigler, Continuous record of microparticle concentration and size distribution in the central Greenland NGRIP ice core during the last glacial period, *J. Geophys. Res.*, *108*(D3), 4098, doi:10.1029/2002JD002376, 2003.

1. Introduction

[2] Ice cores provide a wealth of paleoclimatic information including records of windblown mineral aerosol (hereinafter dust). Among all deposited components this atmospheric constituent has a special quality because not only its concentration but also the size distribution of its insoluble fraction is preserved. As East Asian deserts have been identified as the dominant source area for dust transported to Greenland [*Biscaye et al.*, 1997; *Kahl et al.*, 1997; *Svensson et al.*, 2000; *Bory et al.*, 2002], archives may hold specific information about atmospheric transport in particular. Particulates found in Greenland ice overwhelmingly derive from the insoluble fraction of dust (hereinafter particles) [e.g., *Thompson*, 1977].

[3] Dust concentrations in ice cores vary by a factor of ≈100 between the Holocene and the Last Glacial Maximum (LGM) in central Greenlandic ice [*Steffensen*, 1997; *Fuhrer et al.*, 1999]. Continuous particle and Ca^{2+} measurements in the Renland ice core [*Hansson*, 1994] and continuous Ca^{2+} measurements in the GISP2 and GRIP ice cores [*Mayewski et al.*, 1994; *Fuhrer et al.*, 1999] have shown that during rapid climatic transitions the dust concentration varied synchronously with the $\delta^{18}O$ temperature proxy. Explana-

[1]Also at Alfred-Wegener-Institute for Polar and Marine Research, Bremerhaven, Germany.

0148-0227/03/2002JD002376$09.00

tions for the pronounced increase in dust concentration in cold periods include changed atmospheric conditions [*Petit et al.*, 1981, 1990] and intensified sources [*Fuhrer et al.*, 1999]. Further specification of this general inference, however, remains difficult as the observed dust concentrations are a combined result of a number of entangled mechanisms ranging from dust mobilization in the source areas over uplift and long range transport to deposition onto the ice sheet. *Fuhrer et al.* [1999] discussed some of the relevant processes, but the fact that changes of source aridity, surface wind speed, uplift, transport, and deposition may all have varied jointly on similar timescales [*Porter and Zhisheng*, 1995; *Wang et al.*, 2001] makes it very difficult to assess their relative importance. As yet, only limited clarification can be expected from modeling approaches because current dust models, although having improved considerably, still are unable to reproduce accurately the change in dust concentration observed in polar ice cores and cannot confidently resolve the individual processes involved [*Andersen et al.*, 1998; *Mahowald et al.*, 1999; *Tegen and Rind*, 2000]. Also, models do not provide an adequate description of the mixing mechanisms in the lower atmospheric boundary layer over ice sheets which play an important role in dust deposition.

[4] Size distribution measurements on particles in polar ice cores have shown that the bulk of the particle volume can be described by a single lognormal distribution with a modal diameter around 1.5 to 2.0 μm [*Royer et al.*, 1983]. This mode is found to be fairly robust in remote regions worldwide [*Zdanowicz et al.*, 1998]. But small systematic shifts have been observed on various timescales in ice cores from Greenland as well as from Antarctica [e.g., *Steffensen*, 1997; *Delmonte et al.*, 2002]. As particle size distributions may be indicative of atmospheric transport times it may be possible to use this information to gain further insights into the past dust cycle. But size distribution measurements are scarce. So far they have been performed only in a discontinuous spot check manner using microscopy or the well established Coulter counting technique. For Greenland, *Steffensen* [1997] found a tendency towards larger modal diameters for colder climates, which are also associated with higher dust concentrations in ice cores.

[5] The interpretation of particle size measurements is not straightforward. Dry and wet removal during long range transport is generally size fractionating [*Junge*, 1977]; as well, in-cloud processing may occur [*Wurzler et al.*, 2000], and particles may be further size-fractionated on transfer from air to snow [*Unnerstad and Hansson*, 2001]. Quantification of these processes is difficult, and our current understanding about how different climatic situations may have influenced the particle size distribution is limited. Also, the forward modelling of particle size distributions is not very accurate. Dust modules for general circulation models (GCM) work with one or only few size classes (e.g. four classes covering the range from 1 to 100 μm [*Tegen and Fung*, 1994]) and cannot resolve fine shifts of the mode.

[6] So far, no continuous ice core record of particle size distribution covering the last glacial period has been published. Here we present a comprehensive particle profile from the North Greenland Ice Core Project (NGRIP) deep ice core, drilled at (75.1N, 42.3W) in central Greenland about 300 km north of the summit region. The record is from 1405 m to 2930 m depth and spans the period from ≈9.5 kyr to ≈100 kyr before present (bp), i.e. it includes the Pleistocene to Holocene transition and most of the last glacial period. The core was analyzed continuously for insoluble particle concentration and size distribution using a new laser based sensor coupled to a continuous flow system. To interpret the observed changes in particle size, we present a simple model picture that describes the modification of a particle size distribution during long range transport and deposition.

2. Methods

2.1. Measurements

[7] The measurement procedure and the laser based particle detector have already been described by *Ruth et al.* [2002] and therefore are only briefly outlined here. However, the particle size calibration will be covered in greater detail. The measurements took place in a warm laboratory (18°C) during the NGRIP-2000 field campaign. Continuous sections of ice core were melted in a controlled fashion along the core direction, and the melt water was passed through established continuous flow analysis (CFA) systems [e.g., *Röthlisberger et al.*, 2000; M. Bigler, dissertation in preparation, University of Berne] and to a particle counter. For decontamination purposes the abutting faces of the core sections were carefully cleaned using a stainless steel microtome blade. In addition, the melter had two concentric sections, and only the uncontaminated meltwater from the inner section was used for the analyses as described by *Röthlisberger et al.* [2000]. Peristaltic pumps and teflon tubings were used to feed the water into the detection units. Debubblers were used to eliminate air bubbles.

[8] In our measuring procedure the size distribution data were accumulated over 1.65 m intervals (corresponding to approximately 35–200 yr, see below), while the particle concentration also was recorded at an effective depth resolution of 1.0 cm [*Ruth et al.*, 2002]. Count rates were converted to concentrations using regular flow rate measurements. To avoid coincidence distortion of the particle counting the sample flow of glacial age ice was reduced to approximately 0.15 ml min^{-1}; however, to maintain an optimal flow rate of 1.5 ml min^{-1} through the detector the sample was added to prefiltered (0.2 μm) carrier water (dilution). Dilution was performed below 1494.9 m depth, i.e. for ice from the Younger Dryas period and older; in this case, the volume of ice core liquid consumed for each 1.65 m section was approximately 6 ml.

2.2. Size Calibration of the Particle Sensor

[9] The particle detection is based on laser light attenuation by single particles. The sample water is pumped through an illuminated detection cell, where each particle is detected as a negative peak of transmitted light. The peaks are counted and sorted by height into channels, that can be adjusted to appropriate size intervals. Twelve channels were used in this application.

[10] The interrelation of peak height and particle size is complex as both geometric shadowing and scattering processes are involved. Shadowing depends on geometric particle cross section, and therefore on a combination of

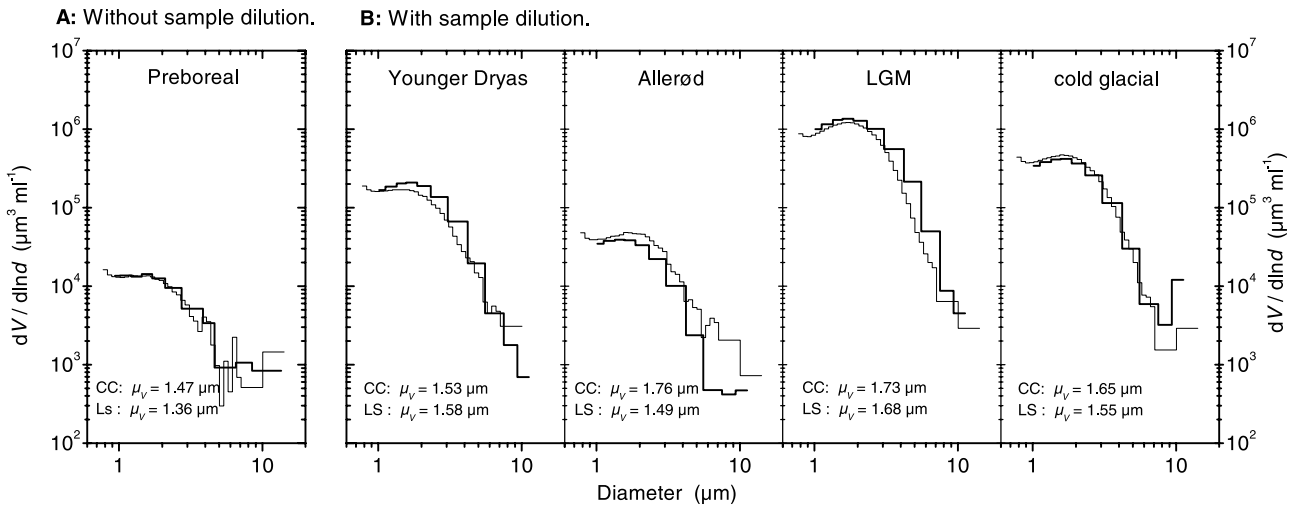

Figure 1. Size distributions by volume used for calibration. Coulter Counter (CC) data in thin lines, laser sensor (LS) data in bold lines. The laser sensor data is shown after the adjustment of its size axis. The rise at the left end of the Coulter Counter curves is due to noise as the lower size limit is reached. Listed is also the lognormal mode µ of the distributions as derived from CC and LS data. Calibration for measurements without sample dilution is based on the Preboreal sample (A); calibration for measurements with sample dilution is based on the other four samples (B).

particle volume, shape and orientation. Scattering in addition depends on optical particle properties and features nonlinearities between particle size and scattered light intensity. Only for particles larger than ≈7 µm diameter geometric shadowing dominates enough to allow a calibration with latex spheres of known diameter. In the remaining main part of the spectrum scattering becomes increasingly important, and a size calibration with latex spheres is inaccurate because dust particles have different scattering properties than latex spheres of identical volume, predominantly due to their nonspherical shape [*Saey*, 1998].

[11] Therefore, a size calibration was achieved indirectly through comparison with measurements obtained using a Coulter Counter, which measures the particle volume directly and independently of shape. At selected depths, NGRIP ice core samples were also measured with a Coulter Counter, and the laser sensor size axis was adjusted until the laser sensor and Coulter Counter data showed optimal correspondence. Samples from five different climatic periods (Preboreal Holocene, Younger Dryas (YD), Allerød, LGM, and pre-LGM cold glacial (CG)) were used for the calibration, thus the full concentration range was covered. Hereby the lower detection limit was recognized at 1.0 µm diameter, and proper sizing showed possible between 1.0 and 11 µm. The total particle concentrations agreed within approximately 5% to Coulter Counter measurements.

[12] During the calibration process it was discovered that the dilution setup had had a modifying influence on the size distribution, probably due to coagulation of particles in a mixing cell with turbulent flow. Therefore, the measurements of Preboreal Holocene ice (undiluted) and glacial age ice (diluted) were calibrated separately. Figure 1 shows the volume distribution spectra used for the two calibrations. The Preboreal sample was used to calibrate the measurements above 1494.9 m depth, that were done undiluted (A). For the calibration of the measurements below this depth the other four samples were used altogether for one separate calibration (B). After the adjustment of the laser sensor size axis, the data sets of the two counters show good accordance. Differences between the laser sensor and the Coulter Counter data may result from the fact that the Coulter Counter data covers only 0.55 m out of the 1.65 m long section measured with the laser sensor so that the underlying size distributions possibly indeed slightly differed in the respective samples. For calibration (B) the differences in the underlying sample populations may be expected to counterbalance each other as several samples could be used for one calibration.

2.3. Data Parametrization

[13] A lognormal function was used to parametrize the volume distribution data:

$$\frac{dV}{d\ln d} = \frac{V_0}{\sqrt{2\pi}\ln\sigma} e^{-\frac{1}{2}\left(\frac{\ln d - \ln\mu}{\ln\sigma}\right)^2},$$

where V_0 is the amplitude, µ the mode and σ the standard deviation of the distribution. Because the width of the size channels was quite large the fit procedure iteratively accounted for the modeled distribution within each channel. Furthermore, the relative quadratic error was minimized thus assigning equal weights to all channels. The first nine channels were considered for fitting, i.e. particles between 1.0 µm and 7.5 µm diameter.

[14] Other parameters are sometimes used to characterize a particle size distribution: The volume V_c of coarse particles ($d > d_c$) is used as well as the relative coarseness as V_c/V_{tot}; d_c was chosen as 7.5 µm in our study. The parameters 'mean volume diameter' (MVD) and 'mean number diameter' (MND) as e.g. used by *Zielinski* [1997] denote the mean diameter with respect to volume or number. These parameters highly depend on the covered size range and thus are intercomparable only for identically treated data sets. Furthermore, the MVD was found to be ambiguous in our data:

At high concentrations it tended to be in phase with changes of the mode μ and in antiphase with the relative coarseness (i.e. it depended on the size of small particles); yet at low concentrations it tended to be in antiphase with the mode and in phase with relative coarseness (i.e. it depended on the abundance of large particles). For these reasons, neither MND nor MVD are used in this study.

[15] Because a considerable portion of the mass is contributed by the small particles below the detection limit of approximately 1.0 μm, mass concentrations reported in this paper are derived as follows: For $d > \mu$ the total measured particle volume $V_m^{d>\mu}$ is taken by summation of all relevant channels or fractions thereof; for $d < \mu$ the volume is taken from the fitted lognormal distribution, i.e. $V_{tot} = V_m^{d>\mu} + 0.5 \cdot V_0$. Subsequently, the total mass concentration is inferred by assuming a material density of 2.6 g cm^{-3} [*Sugimae*, 1984].

2.4. Measurement Errors

[16] Occasionally, sections were affected from system malfunction and were excluded from further processing. A few sections showed a very high concentration of large particles possibly resulting from contamination and were also excluded. The measurement blank for small particles was below 15% of the count rate for most low concentration samples and was negligible in high concentration samples. For coarse particles ($d > 7.5$ μm) the blank relative to sample count rates was higher and more variable; since for these particles counting statistics also deteriorate, caution must be taken when interpreting the volume of the coarse fraction. The error on the total number concentration for all particles is predominantly due to flow rate uncertainties and is estimated to typically 5%–10%. The uncertainty of total volume or mass concentration as due to flow rate and size calibration uncertainties is estimated to be about 15%–20%.

[17] The exact determination of the particle sizes is hindered by the influence of the flow set up on the size distribution, which may not be constant and therefore not at all times be fully compensated for by the calibration. Further, the calibration is affected from the fact that the Coulter Counter data covers only part of the sample population measured with the laser sensor, which may explain the difference of about 0.1 μm between the fit parameter μ when derived from the Coulter Counter or the laser sensor data (see Figure 1). The difference in μ that result from using calibration A or B for any given sample was typically around 0.04 μm. The analytical uncertainty of the fit is variable and lies in the range from 0.01 μm to 0.1 μm diameter. We therefore estimate the possible error for μ to be generally around 0.1 μm diameter; it may be larger for the Holocene samples, where only one calibration sample exists and also the uncertainty of the fit is large. Double measurements on ice from the YD-Holocene transition, one time performed without and the other time with the dilution setup, yielded a discrepancy in μ of up to 0.1 μm, which supports the above estimates.

3. Results

3.1. Size Distributions

[18] Four individual volume size distributions are shown in Figure 2 for illustration. They are representative for different climatic periods, namely LGM (a), Stadial (S) S9 (b), Interstadial (IS) IS10 (c), and Preboreal Holocene (d). The samples span a concentration range of more than two orders of magnitude for particles smaller than 7.5 μm. For coarse particles larger than 7.5 μm the concentration range of the four samples is less than one order of magnitude and is not strictly correlated to the concentration of small particles.

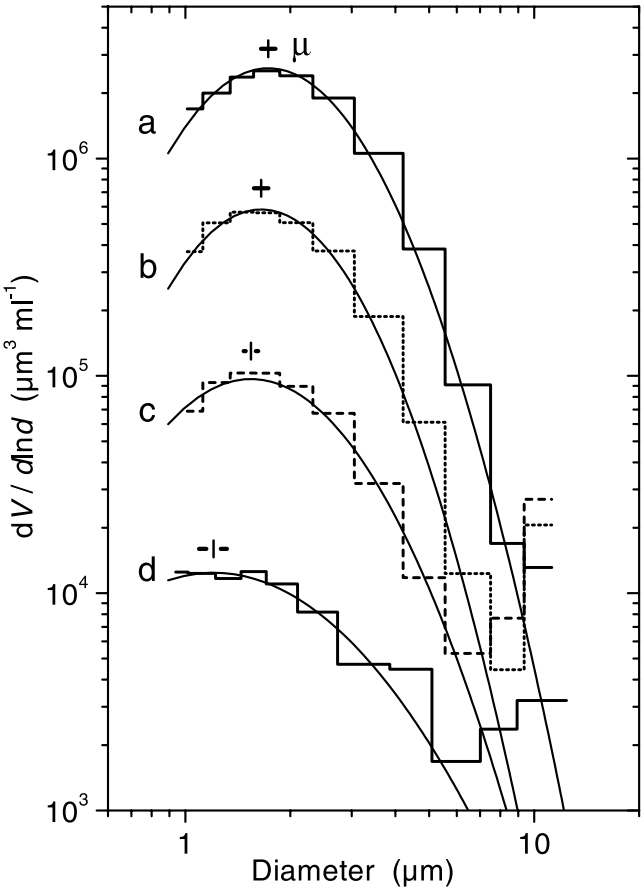

Figure 2. Individual size distributions by volume from different climatic periods along with lognormal fits. a: 1831.50–1833.15 m (LGM); b: 2075.70–2077.35 m (S9); c: 2121.90–2123.55 m (IS10); d: 1460.25–1461.90 m (Preboreal). Indicated is the position of the mode and the uncertainty of the fit [a: (1.73 ± 0.02) μm; b: (1.65 ± 0.06) μm; c: (1.54 ± 0.05) μm; d: (1.21 ± 0.11) μm].

[19] The respective lognormal fits are also shown in Figure 2, and the position and uncertainty of the mode μ are indicated. The fits describe the measured distributions very well for high concentration samples. For low concentration samples the description is still satisfactory, however deviations of the data from the ideal model distribution are larger. It may also be noticed that with higher concentrations the mode tends to get coarser whereas the width of the distribution tends to decrease.

3.2. Profiles

[20] Particle concentration and size distribution parameters of all samples are plotted as depth profiles in Figure 3. Shown are the insoluble particle number concentration C_N, mass concentration C_M, lognormal mode μ of the volume distribu-

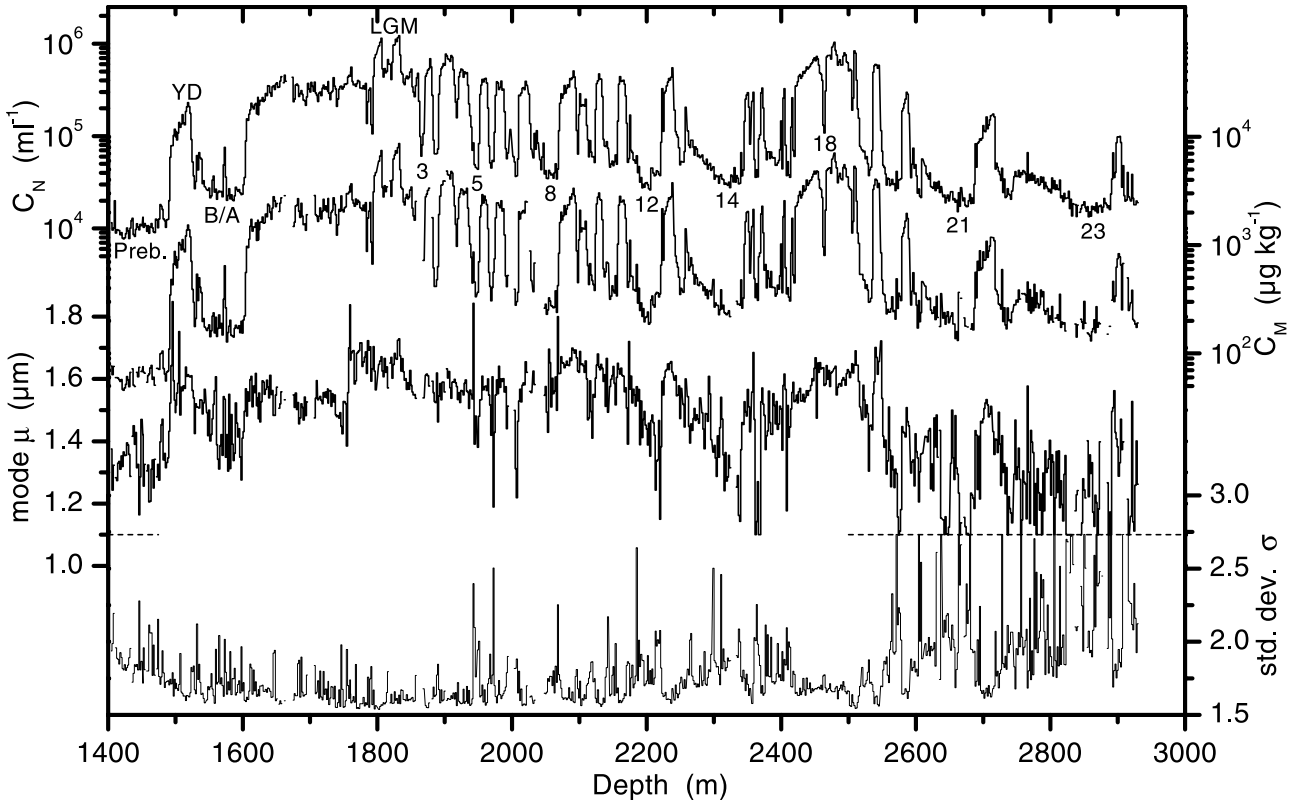

Figure 3. Profiles of microparticle concentration and lognormal size distribution parameters µ (diameter) and σ. Number concentration is based on counts of particles larger 1.0. Gaps arise either from missing data or from data that did not allow for a proper lognormal fit. Selected climatic periods are labeled: Preb = Preboreal Holocene, YD = Younger Dryas, B/A = Bølling/Allerød, LGM = Last Glacial Maximum; numbers refer to Dansgaard/Oeschger-events. The data of the bottom two panels was truncated at the dashed line indicated.

tion, and lognormal standard deviation σ. The concentration profiles clearly exhibit all climatic events known from the Greenlandic GRIP and GISP2 deep ice core records [*Johnsen et al.*, 1997; *Grootes and Stuiver*, 1997], some of which have been labeled in the figure. In particular, the stadial-interstadial fluctuations (or Dansgaard-Oeschger (D/O)-events) are clearly resolved. Periods of low particle concentrations correspond to warm phases while cold phases correspond to high particle concentrations. Concentrations are lowest during Preboreal Holocene ($C_N \approx 1 \cdot 10^4$ ml^{-1} or $C_M \approx 70$ µg kg^{-1}) and highest during LGM ($C_N \approx 1 \cdot 10^6$ ml^{-1} or $C_M \approx 8000$ µg kg^{-1}). This compares well to the reported particle mass concentrations from the GRIP core of 50 µg kg^{-1} and 8000 µg kg^{-1} for Preboreal and peak-LGM respectively [*Steffensen*, 1997]; discrepancies may be due to differences in the methods of measurement and data evaluation and need not be of geographical origin. The relative changes of the mass concentrations we observe across D/O-transitions range from a factor of 5 to 18 and are typically around 8.

[21] As expected, the overall appearance of the particle concentration profile closely resembles the continuous Ca^{2+} concentration profile from the GRIP core [*Fuhrer et al.*, 1999]. This means that the soluble and insoluble fractions of dust varied largely alike. However, systematic changes of the Ca^{2+}/particle ratio by a factor ≤ 2 have been observed [*Steffensen*, 1997; *Ruth et al.*, 2002].

[22] The close correspondence of the particle profile to the GRIP Ca^{2+} or $\delta^{18}O$ profiles permits to establish a provisional timescale for our NGRIP particle profile by matching respective climatic events and transferring the GRIP SS09 timescale [*Johnsen et al.*, 1997] to the NGRIP core. Thereby we infer that the time spanned by each 1.65 m section ranges from 35 to 200 years. We also infer that the concentration changes at D/O-transitions may have happened within 100 years or less.

[23] The mode µ of the particle size distribution shows considerable systematic variability throughout the record, and most major climatic events as identified from the concentration profiles are also visible in the size distribution. These are, in particular, the YD and B/A periods, and the most prominent D/O-events; but also smaller D/O-events or the LGM as a whole are identifiable in the profile. Typical values for µ in the Preboreal are around 1.3 µm diameter; and peak values exceed 1.7 µm during LGM. Typical values within the Pleistocene are around 1.6 µm during cold periods and may decrease to values around 1.4 µm or less during interstadial warm periods. A marked increase of the mode can be noticed between 2600 m and 2500 m depth, which corresponds to the transition from Marine Isotope Stage (MIS) 5 to MIS 4. Below this depth (i.e. during MIS 5) µ is generally about 0.2 µm smaller than above. During corresponding periods

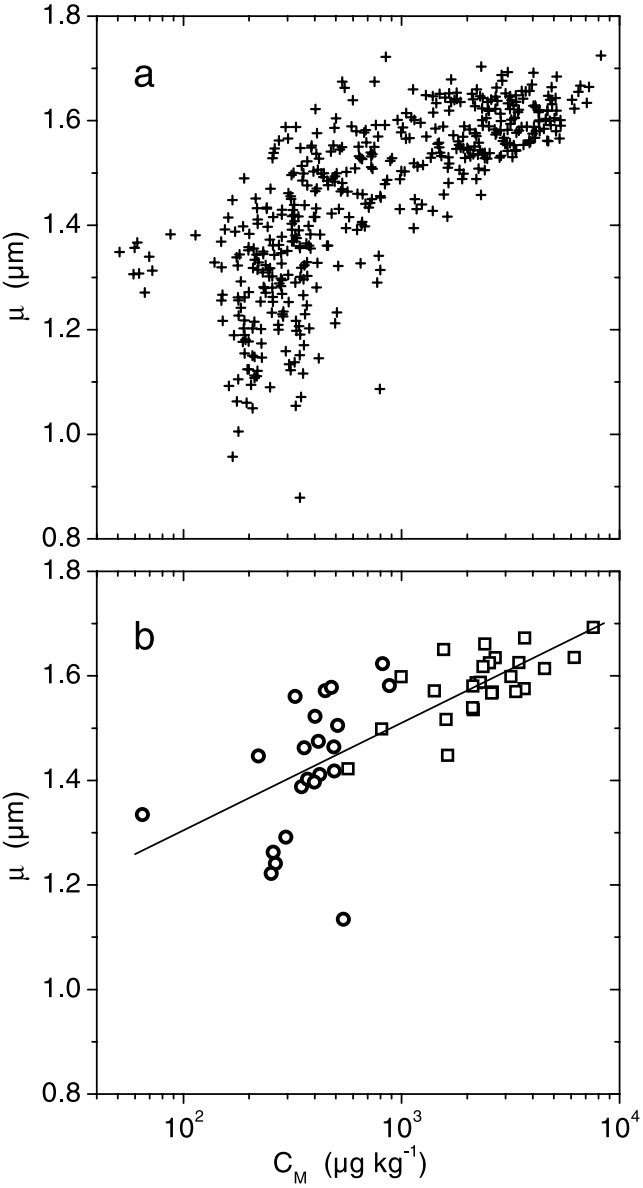

Figure 4. Correlation of the mode μ and the mass concentration C_M. a: All data has been averaged such that each data point represents 200 years. b: All data has been averaged over climatic periods; circles denote warm periods, squares denote cold periods. A logarithmic trend line is also shown.

we find modes that are smaller than those of *Steffensen* [1997] by 0.2 μm.

[24] The switching of the mode between states may happen as fast as the concentration changes, but it is not always as evident. Further, μ tends to be more variable (point-to-point variation) when dust concentrations are low. This higher variability persists even when the data are averaged over equally long time periods; so it is not a consequence from formal counting statistics nor from the fact that low concentration samples systematically cover shorter time spans.

[25] The lognormal standard deviation also shows systematic variations. It ranges from about 1.55 during LGM to more than 2 during the warm periods of MIS 5 (below 2550 m depth). This indicates that in warm climates the mode was more variable *within* the 35–200 year period covered by each 1.65 m section. At these times μ shows a large point-to-point variability, which suggests increased variability also on longer timescales, however only with marginal significance.

3.3. Systematic Changes of the Mode

[26] Figure 3 shows that the mode tends to increase with larger particle concentrations. A systematic plot of these two parameters is shown in Figure 4a, where data are averaged to 200 years resolution to reduce the point-to-point scatter for periods with higher layer thickness (and thus less time spanned by each sample). A clear positive correlation is exhibited. It also can be noted that the spread of the mode is smaller by a factor of 3 for high compared to low particle concentrations. Coarser modes and smaller spread for high concentration samples are also observed if the data are averaged over climatic periods (Figure 4b).

3.4. Detailed Profile Section

[27] A closer look at rapid transitions may bring further insights into the dust regime. Figure 5 shows the enlarged profile from IS 9 through IS 12 with size distribution parameters, particle concentration, and $\delta^{18}O$ (isotope data: personal communication from NGRIP-members, unpublished data). Cold periods very clearly show high particle concentrations and vice versa. Further, almost all high concentration periods are concurrent with large modes;

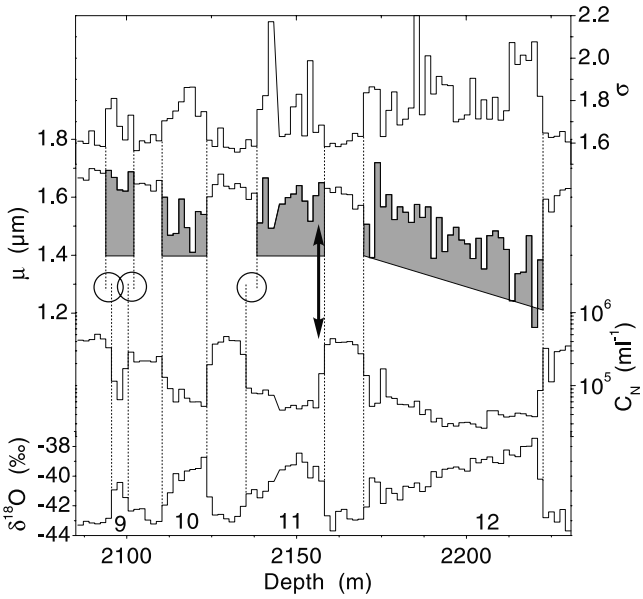

Figure 5. Detail from profiles showing various rapid D/O-transitions. Shown are size distribution parameters σ and μ, number concentration C_N, and $\delta^{18}O$ (data is personal communication from NGRIP-members). Shaded areas emphasize interstadials as inferred from the profiles of μ and σ. Circles mark instances where the timing of a transition may be inferred differently from μ and σ or respectively from V_N and $\delta^{18}O$. The arrow points to a transition where μ seemingly shows other timing than σ and C_N. Numbers in the bottom panel indicate interstadials.

however, not all periods with low concentrations are accompanied by smaller modes, and during low concentration periods the mode is more variable. This shows an independence of μ and V which is especially pronounced during warm periods.

[28] The fact that the mode is more variable during warm periods may cause confusion when determining the exact point of a transition. One such occasion at the beginning of IS 11 is marked in Figure 5 with an arrow. Here, the size distribution shifts synchronously with the concentration into the ''warm''-state as can be seen from the profile of σ. However, its increased variability allows the mode to stay large for two more samples (corresponding to roughly 200 years). Only the increased values for σ show that the individual dust events contributing to the multiyear samples were already more variable with respect to particle size, as is typical for warm periods. Therefore, D/O-transitions seem to show more clearly in σ than in μ.

[29] Another observation is that there may indeed be a difference in the particular time when a transition occurs in the concentration and in the size distribution of particles (circles in Figure 5). No systematic leads or lags seem to occur, but shifts range up to ±200 years. This again shows some independence of the processes influencing the particle concentration or size distribution. The independence is observed especially during warm periods, and it vanishes if the data are averaged for several centuries.

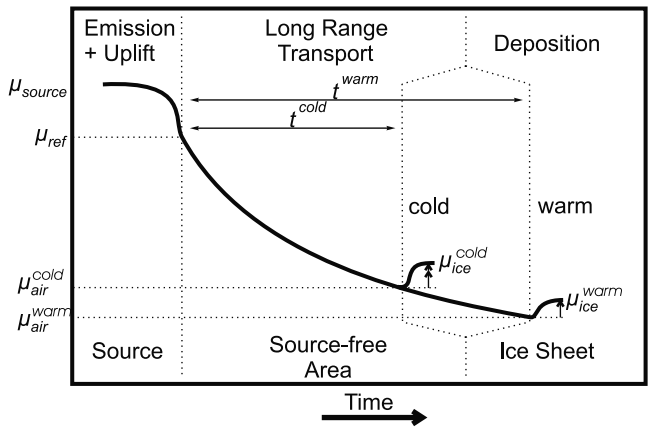

Figure 6. Conceptual illustration of the model picture. The airborne particle size distribution with mode μ_{source} at the source is changed rapidly during uplift until μ_{ref} is reached. Here, per definition, long range transport across source-free areas starts. During long range transport the mode decreases slowly owing to size fractionating depletion processes. Because the transit time t during cold climates is shorter than during warm climates the mode μ_{air} of airborne particles at the ice sheet is larger during cold climates. During deposition the mode is shifted slightly towards larger particles leading to μ_{ice}. Upper indices '*cold*' and '*warm*' denote cold and warm climatic states, respectively.

4. A Simple Model Picture

[30] The atmospheric dust cycle starts with the production of wind-erodible material in the source areas by weathering processes [*Pye*, 1987]. The amount of dust entrained into the atmosphere depends on the frequency and strength of surface winds [*Gillette et al.*, 1980], the mobility of the dust, and the size of the source areas. The geographical overlap of source regions and long range transport zones may be another important factor [*Chylek et al.*, 2001]. The transport of dust depends on long range atmospheric circulation patterns, which in turn are influenced by e.g. global heat distribution or the ice cover of land and ocean [*Krinner and Genthon*, 1998]. Transport efficiency depends on processes removing aerosol en route. Finally, air-to-snow transfer of dust depends on wet and dry deposition processes [*Davidson et al.*, 1996].

[31] From ice cores and from other paleoclimatic archives it has been inferred that atmospheric circulation during the last glacial period differed from present day's [e.g., *Janecek and Rea*, 1985; *Rea*, 1994; *Kapsner et al.*, 1995; *Lamy et al.*, 1999; *Lagroix and Banerjee*, 2002]; in particular, an increased westerly flow has been proposed for both the northern and the southern hemispheres. On the hypothesis that transit times control the size distribution, we will estimate in the following the degree to which transport needs to have been faster to explain the observed size changes of particles. First however, we will investigate the extent to which the observed changes may be due to changed deposition conditions during different climates. Hereby, our very simple approach clearly is far from capturing reality in its complexity; but at least the direction of the various effects and rough estimates of their magnitudes may be attained.

[32] For comparison of two climatic states in the following sections we use the upper index '*cold*' to denote a cold state and the upper index '*warm*' to denote a warm state. A conceptual illustration of our model picture sketched in Figure 6.

4.1. Size Fractionation During Deposition

[33] Particles are transferred from the air to the snow by dry and wet deposition [see, e.g., *Alley et al.*, 1995]. Wet deposition includes all precipitation related events and is described by an effective wet deposition velocity v_w. Dry deposition processes include all sinks not directly related to precipitation, i.e. mainly sedimentation, impaction, and snow drift scavenging, and are summarized as an effective total dry deposition velocity v_d. We consider only multiyear means (disregarding e.g. changed seasonality of precipitation [*Werner et al.*, 2000]) and assume that the precipitation rate equals the accumulation rate; then the deposition flux f may be expressed as $f = (v_w + v_d)\, c_{air} = (\varepsilon A + v_d)\, c_{air}$ with

ε: scavenging ratio, i.e. particle concentration in new snow divided by c_{air},
A: snow accumulation rate (in water equivalent), and
c_{air}: airborne particle concentration.

[34] As a first order approximation particle size fractionation by dry deposition may be described by $v_d = kd^n$ (d: particle diameter, k and n: constants), although for large particles v_d may be rate limited through insufficient vertical mixing. Wet deposition may be regarded as so efficient that at least for sufficiently high precipitation rates its size fractionating potential [*Junge*, 1977] is canceled; thus we assume ε independent from particle size. In this picture the size distribution is shifted towards larger particles by dry

deposition but not by wet deposition; consequently the degree of modification depends on the ratio of dry and wet deposition fluxes. Therefore, a change in the snow accumulation rate will change the archived particle size distribution [see also *Unnerstad and Hansson*, 2001].

[35] Assuming a unimodal, lognormal distribution defined by $\langle \mu_{air}, \sigma \rangle$, the size distribution of particles in the air will transform during deposition as $\langle \mu_{air}, \sigma \rangle \cdot (v_w + v_d)$. The mode μ_{ice} of the size distribution in the ice is found at the maximum of this product and is given by

$$\ln\left(\frac{\mu_{ice}}{\mu_{air}}\right) = n\sigma_g^2 \frac{v_d}{v_w + v_d} = n\sigma_g^2 \frac{k\mu_{ice}^n}{A\varepsilon + k\mu_{ice}^n}$$

where $\sigma_g = \ln \sigma$. The maximum shift in modal particle size occurs if only dry deposition is active. In that extreme case $\frac{\mu_{ice}}{\mu_{air}} = \exp(n\sigma_g^2)$; and with $n = 2$ (sedimentation) and $\sigma = 1.7$ a ratio of $\approx$1.7 is obtained.

[36] Because the accumulation rate varied under different past climates the particle size distribution shifts during deposition were also different. To calculate the size shift for two different accumulation rates we choose $\mu_{air} = 1.4$ μm and assume constant values for n ($n = 2$), σ ($\sigma = 1.7$), k ($k = 8.3 \cdot 10^7$ m^{-1}s^{-1} from *Fuchs* [1964]), and ε. The values vor ε are not well known, but $0.2 \cdot 10^6 \leq \varepsilon \leq 2.0 \cdot 10^6$ seems probable as *Davidson et al.*, [1996] find $\varepsilon = (0.65 \pm 0.31) \cdot 10^6$ for Ca^{2+} at Summit. For $A^{warm} = 0.2$ ma^{-1} and $A^{cold} = 0.5\ A^{warm}$, which reflects LGM vs. Preboreal accumulation changes [*Johnsen et al.*, 1997], we obtain a difference $\Delta = (\mu_{ice}^{cold} - \mu_{air}^{cold}) - (\mu_{ice}^{warm} - \mu_{air}^{warm})$ of $\Delta = 0.08$ μm for $\varepsilon = 0.2 \cdot 10^6$ and $\Delta = 0.01$ μm for $\varepsilon = 2.0 \cdot 10^6$, which typically is about 1/4 of the absolute shifts $\mu_{ice} - \mu_{air}$ in our calculations. Similar results are achieved if more realistic calculations of v_d are used [*Sehmel*, 1980].

[37] These calculated differences only account for roughly 3% to 20% of the observed change of μ of μ_{ice} of approximately 0.4 μm. We therefore conclude that the observed differences of μ during different climatic periods predominantly result from changed airborne size distributions over Greenland. This also holds true if typical coatings of soluble salts (e.g. $CaCO_3$) are assumed around the airborne particles.

4.2. Size Fractionation During Emission and Long-Range Transport

4.2.1. Emission

[38] Surface wind speed mainly influences the abundance of particles greater than 10 μm diameter but has little effect on the size distribution of particles that may be carried long distances [*Gillette et al.*, 1974; *D'Almeida and Schütz*, 1983]. Because we consider only particles smaller than 10 μm we therefore assume that the size distribution of airborne particles above the ground is independent from the source strength. The mode of this distribution be μ_{source}.

4.2.2. Long-Range Transport

[39] The change of particle concentration during long range transport can be described by the term $f \cdot e^{-t/\tau}$, with

t: transit time between free troposphere at source and deposition onto the ice sheet

τ: residence time governed by depletion processes en route, and

f: correction factor in our one-dimensional approach to account for external mixing with particle free air (dilution).

We assume $\tau(d) = \frac{H}{\tilde{v}_w + \tilde{v}_d}$, where H denotes the mixing height, $\tilde{v}_w$ describes the depletion process en route due to wet depletion and $\tilde{v}_d$ due to dry depletion. Dry depletion again is assumed to be size fractionating according to $\tilde{v}_d = kd^n$, and $\tilde{v}_w$ again is assumed to be so efficient that its size fractionating effect is overridden.

[40] Following the motion of an air parcel $\langle \mu_0, \sigma \rangle$ transforms as $\langle \mu_0, \sigma \rangle \cdot f \cdot e^{-t\frac{\tilde{v}_w + \tilde{v}_d}{H}}$. The resulting distribution is not exactly lognormal; however, the new mode μ is characterized by:

$$\ln\left(\frac{\mu}{\mu_0}\right) = -n \cdot \sigma_g^2 \cdot \frac{t}{\tau} \frac{\tilde{v}_d}{\tilde{v}_w + \tilde{v}_d} \tag{1}$$

which reflects that μ decreases with time during transport. Simultaneously, the distribution gets narrower, i.e. σ_g also decreases. Consequently, the change of μ occurs more rapidly at the beginning, when σ_g is large.

[41] We now compare the size change during long range transport under a cold and warm climatic state starting from a common reference size distribution with the mode $\mu_{ref} = \mu_{ref}^{cold} = \mu_{ref}^{warm}$ in the free troposphere upon uplift. With the assumption of identical initial widths of distributions ($\sigma_g^{cold} = \sigma_g^{warm}$), dry deposition mechanisms ($n^{cold} = n^{warm}$), dry deposition strengths ($\tilde{v}_d^{cold} = \tilde{v}_d^{warm}$), and mixing heights ($H^{cold} = H^{warm}$) the ratio $\frac{\mu_{air}^{cold}}{\mu_{air}^{warm}}$ of the airborne modes at the ice sheet can be deduced from equation 1 as

$$\ln\left(\frac{\mu_{air}^{cold}}{\mu_{air}^{warm}}\right) = -\ln\left(\frac{\mu_{air}^{warm}}{\mu_{ref}^{warm}}\right)\left[1 - \frac{t^{cold}}{t^{warm}}\right] \tag{2}$$

thus linking $\mu_{air}^{cold}/\mu_{air}^{warm}$ with t^{cold}/t^{warm} (Figure 7). Since we have only limited knowledge about μ_{ref}, three different values have been applied for $\mu_{air}^{warm}/\mu_{ref}^{warm}$: All are based on $\mu_{air}^{warm} = 1.3$ μm, which is the average mode we observed for the Preboreal; based on data from *D'Almeida and Schütz* [1983] and *Wagenbach and Geis* [1989] μ_{ref}^{warm} has been taken as 2.5 μm, 3.2 μm and 4.0 μm respectively.

[42] In Figure 7 typical ratios of $\mu_{air}^{cold}/\mu_{air}^{warm}$ as based on our measurements have been marked for LGM vs. Preboreal and Stadial vs. Interstadial after a 10% correction for different deposition scenarios was made. With the assumption that differences in long range transport account for these size changes the implied ratio of transit times can be read from Figure 7. Our model suggests $t^{cold}/t^{warm} \approx 0.75$ for the LGM vs. Preboreal and $t^{cold}/t^{warm} \approx 0.9$ for the Stadial vs. Interstadial comparisons respectively. These reasonable values support the hypothesis that a variable transit time may indeed have caused the observed particle size changes.

4.3. Implications From Size Changes for Concentration Changes

[43] The estimated ratio of transit times t^{cold}/t^{warm} imposes limits on dust concentration change associated with changed long range transport. The concentration change

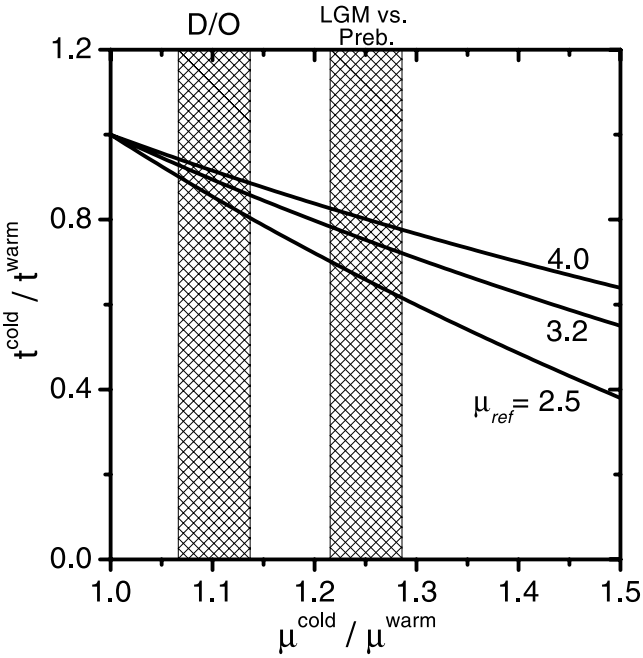

Figure 7. Implications from observed size changes μ^{cold}/μ^{warm} for the change in transit times t^{cold}/t^{warm}. Curves consider different scenarios for μ_{ref}. Shaded areas mark LGM vs. Preboreal and Stadial vs. Interstadial (D/O) changes, respectively.

resulting from varying long range transport between cold and warm periods may be assessed as $(\frac{C^{cold}}{C^{warm}}) = \frac{f^{cold}}{f^{warm}} \cdot \exp(\frac{t^{warm}}{\tau^{warm}}(1 - \frac{\tau^{warm}}{\tau^{cold}}\frac{t^{cold}}{t^{warm}}))$. To calculate C^{cold}/C^{warm} as a function of t^{cold}/t^{warm} a number of parameters must be estimated. For dilution with particle free air $f \sim 1/s$ is taken where s is the transversal width of the airborne dust plume. Assuming $s = \sqrt{D/t}$ and no change of eddy diffusion constants D yields $f^{cold}/f^{warm} = (t^{cold}/t^{warm})^{-1/2}$. The scaling factor t^{warm}/τ^{warm} can be estimated from equation 1 by taking $\frac{\mu}{\mu_0} = \frac{\mu_{air}^{warm}}{\mu_{ref.}^{warm}} \approx \frac{1.3\mu m}{3.2\mu m}$, $n = 2$ (sedimentation), $\sigma_g = \ln 1.7$, and by assuming $\tilde{v}_d \approx \tilde{v}_w$ during warm climates, which renders $\frac{t^{warm}}{\tau^{warm}} = 3.2$.

[44] In Figure 8 the resulting C^{cold}/C^{warm} is shown as a function of t^{cold}/t^{warm} for two different assumptions of τ^{warm}/τ^{cold}: First, $\tau^{warm}/\tau^{cold} = 1$ is taken for curve (A), i.e. C^{cold}/C^{warm} resulting from changed transit times only. For curve (B) the residence times were also varied, which is more realistic; to estimate τ^{warm}/τ^{cold} in this case it was assumed that $H^{cold} = H^{warm}$, and $\tilde{v}_d^{cold} = \tilde{v}_d^{warm}$; $\tilde{v}_w^{cold}/\tilde{v}_w^{warm}$ was interpolated between 1 (no change) and 0.5 (for LGM vs. Preboreal) to account for reduced wet depletion en route during LGM [*Andersen and Ditlevsen*, 1998]. This leads to $\tau^{Preb}/\tau^{LGM} = 0.75$ and gives values for C^{cold}/C^{warm} of ≈ 5 for LGM vs. Preboreal and ≈ 2 for a typical D/O transition.

[45] Compared to the observed concentration increases in our data of 100-fold from Preboreal to LGM it is evident even from our rough estimate that other processes must have contributed more effectively to the concentration increase than did changes of atmospheric circulation. These other processes may have included source strength intensification through an increased frequency of dust storms, higher surface wind speeds or increased source aridity, as these do not cause a change of the size distribution.

[46] The increase of airborne dust concentration due to higher wind speed and a reduced hydrological cycle during the LGM compared to present day has been calculated by *Andersen and Ditlevsen* [1998] as well as *Tegen and Rind* [2000]; their calculations suggest increases of 2-fold and 4-fold, respectively. The similarity of these values to our own estimates, which are based only on the observed size changes and a number of independent assumptions, supports the hypothesis that changes in transit times may have controlled the size distribution of microparticles in polar ice cores.

5. Comparison With Other Ice Core Records

[47] Much attention has been given to the question "whether particles were larger during Holocene or LGM". However, this unspecific formulation allows for several confusions. Firstly, the answer depends on the size parameter considered because various size parameters behaved differently. In our data set we find instances where, for example, the mode increases, absolute coarseness stays unchanged, relative coarseness decreases, and the mean volume diameter remains unchanged. Therefore, the size parameter considered must always be specified. Secondly, the stated question may be confused with the one "whether particles were larger in conjunction with high

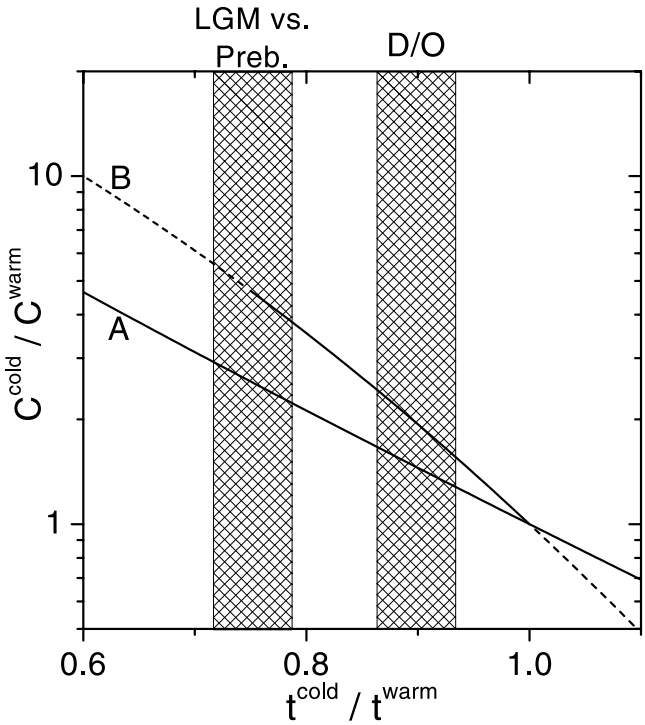

Figure 8. Proposed concentration change C^{cold}/C^{warm} as a function of changed transit time t^{cold}/t^{warm} for two scenarios of τ^{cold}/τ^{warm}. (A): no change of residence times; (B): reduction of wet removal during LGM as described in the text; extrapolations are dashed. Shaded areas mark probable values for t^{cold}/t^{warm} for LGM vs. Preboreal and D/O transitions as inferred from Figure 7.

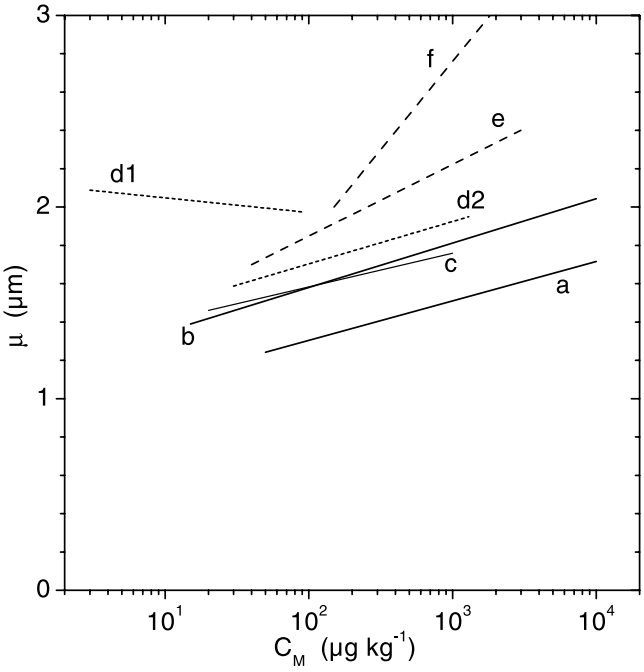

Figure 9. Correlation of C_M and μ in different ice cores from Greenland (solid lines) and from Antarctica (broken lines). a: NGRIP (this work); b: GRIP [*Steffensen*, 1997]; c: Dye3 [*Steffensen*, 1995]; d1: EPICA Dome-C, Holocene data until mid-transition (younger than ≈14.5 kyr bp) [*Delmonte et al.*, 2002]; d2: EPICA Dome-C, glacial age data starting mid-transition (older than ≈14.5 kyr bp) [*Delmonte et al.*, 2002]; e: Dome-C (Holocene and glacial samples) [*Petit et al.*, 1981]; f: Vostock (Holocene and glacial samples) [*De Angelis et al.*, 1984]. For (e) and (f) mass concentrations were inferred from the number concentrations reported using a conversion deduced from *Delmonte et al.* [2002].

or with low particle concentrations"; the necessity for this differentiation has become apparent at least for Antarctica from recent work (see below).

[48] Regarding the dependance of the mode on particle concentration, observations from the Greenlandic Dye3 [*Steffensen*, 1995] and GRIP [*Steffensen*, 1997] ice cores during the last glacial resemble each other closely with respect to both rate of increase as well as absolute level (see Figure 9). In the NGRIP core we find a similar rate of increase, but a lower absolute level, which may be due to methodical or unknown geographical differences. For Antarctica, in early size distribution measurements, *Petit et al.* [1981] and *De Angelis et al.* [1984] did not perform lognormal fits, but their examination of the data suggested increasing modes with increasing particle concentration (Figure 9). Both find this trend for glacial as well as for Holocene samples. However, new Antarctic data by *Delmonte et al.* [2002] contains increasing modes with increasing concentration only for glacial ice older than the Antarctic Cold Reversal (older than ≈14.5 kyr bp). Yet unexplained, the opposite behavior is clearly exhibited for ice younger than ≈14.5 kyr bp; and although particle modes increase with concentration in Pleistocene ice they are still larger during Holocene than during LGM, which may be an important clue for the understanding of past southern hemisphere climate. This probably had not been observed in the earlier Antarctic work [*Petit et al.*, 1981; *De Angelis et al.*, 1984] due to limited number and nonrepresentative selection of samples. For Greenland such a split behavior is not observed based on the very few Holocene measurements published [*Steffensen*, 1997; *Zdanowicz et al.*, 2000]. The larger absolute values of μ in Antarctica compared to Greenland may result from higher contribution of size fractionating dry deposition due to a lower accumulation rate at the Antarctic sites.

[49] Regarding the relative coarseness of particles in ice cores, a greater relative abundance of large particles concurrent with high concentrations had been reported for Antarctica [*Petit et al.*, 1981] but a smaller one for Greenland [*Steffensen*, 1997]. However, like *Steffensen* [1997], also *Delmonte et al.*, [2002] find fewer large particles during times of high concentrations. Since these new data have a higher resolution than those of *Petit et al.* [1981], the disagreement seems to be resolved. Also we find relatively less large particles at high concentrations, so that it seems evident that relative coarseness changed similarly in Greenland and Antarctica. Although findings for Greenland and Antarctica are in accordance at least during the glacial epoch the atmospheric systems transporting dust to the polar ice sheets may have behaved very differently in the northern and southern hemispheres; whereas in Antarctica the abundance of large particles clearly must be driven by atmospheric transport, in Greenland also other causes such as varying contributions of proximal sources or of biological particles may be important.

6. Conclusions

[50] A laser microparticle detector was used for very efficient counting and sizing of windblown dust particles in the NGRIP ice core. A more than 1500 m long continuous profile of particle concentration and size distribution is provided spanning the period approximately from 9.5–100 kyr bp. The laser sensor was easy to handle and proved suitable for field usage. It was possible to calibrate the laser sensor for proper sizing of windblown dust particles. In future usage the flow system between melter and sensor should be as short as possible and kept unchanged throughout the measurements. Calibrations may be achieved indirectly by forced agreement to Coulter counter measurements but should be based on multiple, identical samples from different climatic periods, and should be verified.

[51] We find particle concentrations higher by a factor of 100 during LGM than during the Preboreal and concentration changes by typically a factor of 8 at the sharp transitions of D/O-events. The mode μ of the lognormal size distribution varies systematically with a tendency towards smaller particles during warmer climates. During warmer climates the variability of the mode is higher, and the standard deviation σ also increases. The latter may be due to increased variability of the size distributions in events contributing particles for each multiyear sample.

[52] We base our interpretation of the particle size distribution on a highly simplified, but quantitative model of atmospheric transport and deposition of dust. From this we

suggest the mode of the distribution as indicating atmospheric transit times during transport from the source to the ice sheet. Larger modes may indicate shorter transit times, which may result from higher advection velocities and/or shorter transport routes, i.e. changed atmospheric circulation patterns. Both may be related to changes in the position of the Polar Front. From our data we estimate a ≈25% shorter transit time during LGM than during the Preboreal. We infer that circulation changes alone cannot account for the observed particle concentration increase by a factor of 100. Therefore, other processes such as source intensification might predominately have caused this increase. The synchronism of respective changes in the source areas with changes of large scale atmospheric circulation patterns suggests strong mediating mechanisms.

[53] During warm periods a tendency towards longer transit times is inferred; and transit times were much more variable during these periods. Conversely, atmospheric circulation appears to have been more stable when providing faster transport during cold climates. This may reveal the variability of the Polar Front with respect to the source areas: During cold periods the Polar Front may have always been located far enough south to provide fast transport from the East Asian source areas to Greenland. During warmer periods, the Polar Front may have been located generally further north but was subject to occasional southward excursions.

[54] The variability of transit times during warm periods is - on timescales of up to several 100 years - not connected to concentration changes, which may be controlled by variable source strength. This possible independence between dust production processes and long range transport times may also be evident from occasional timing differences of particle concentration and size distribution parameters at rapid climatic transitions. This supports our notion that source processes by themselves do not influence the size distribution of particles carried to Greenland. It further suggests that source processes and long range transport are two independent results from environmental forcings.

[55] Clearly, the interpretation of particle size distributions in ice cores is limited through inadequate understanding of size fractionating processes. More accurate model calculations for long range transport and particle deposition are needed to check our findings and to draw more differentiated conclusions from the size distribution data. Particle size distribution measurements at high depth resolution may assist the understanding of rapid climate transitions during the last glacial period. Furthermore, closer investigation of size distributions in Greenland during the Holocene are desirable for a comparison to the newest Antarctic results. As insights on variability, timing and the systematics of changes are benefits from continuous measurements, these should always be preferred over discontinuous measurements.

[56] **Acknowledgments.** The North-GRIP project is directed and organized by the Department of Geophysics at the Niels Bohr Institute for Astronomy, Physics and Geophysics, University of Copenhagen. It is being supported by funding agencies in Denmark(SNF), Belgium (NFSR), France (IFRTP and INSU/CNRS), Germany (AWI), Iceland (RannIs), Japan (MECS), Sweden (SPRS), Switzerland (SNF) and the United States of America (NSF). We wish to thank all the funding bodies and field participants. Regine Röthlisberger is acknowledged for her exceptional dedication in running the CFA-lab in the field. Two anonymous reviewers, Hubertus Fischer and John Robbins are thanked for their helpful comments to the manuscript.

References

Alley, R., R. Finkel, K. Nishuzumi, S. Anandakrishnan, C. A. Shuman, G. Mershon, G. A. Zielinski, and P. A. Mayewski, Changes in continental and sea-salt atmospheric loadings in central greenland during the most recent deglaciation: Model-based estimates, *J. Glaciol.*, *41*, 503–514, 1995.

Andersen, K. K., and P. D. Ditlevsen, Glacial-interglacial variations of meridional transport and washout of dust: A one-dimensional model, *J. Geophys. Res.*, *103*(D8), 8955–8962, 1998.

Andersen, K. K., A. Armengaud, and C. Genthon, Atmospheric dust under glacial and interglacial conditions, *Geophys. Res. Lett.*, *25*(13), 2281–2284, 1998.

Biscaye, P. E., F. E. Grousset, M. Revel, S. Van der Gaast, G. A. Zielinski, A. Vaars, and G. Kukla, Asian provencance of glacial dust (stage 2) in the Greenland Ice Sheet Project 2 ice core, Summit, Greenland, *J. Geophys. Res.*, *102*(C12), 26,765–26,781, 1997.

Bory, A. J.-M., A. Biscaye, A. Svensson, and F. E. Grousset, Seasonal variability in the origin of recent atmospheric mineral dust at NorthGRIP, Greenland, *Earth Planet. Sci. Lett.*, *196*, 123–134, 2002.

Chylek, P., G. Lesins, and U. Lohmann, Enhancement of dust source area during past glacial periods due to changes of the Hadley circulation, *J. Geophys. Res.*, *106*(D16), 18,477–18,485, 2001.

D'Almeida, G. A., and L. Schütz, Number, mass and volume distributions of mineral aerosol and soils of the Sahara, *J. Clim. Appl. Meteorol.*, *22*, 233–243, 1983.

Davidson, C. I., M. H. Bergin, and H. D. Kuhns, The deposition of particles and gases to ice sheets, in *Chemical Exchange Between the Atmosphere and Polar Snow*, edited by E. W. Wolff and R. C. Beales, pp. 275–306, Springer-Verlag, New York, 1996.

De Angelis, M., M. Legrand, J. R. Petit, N. I. Barkov, Y. S. Korotkevitch, and V. M. Kotlyakov, Soluble and insoluble impurities along the 950 m deep Vostok ice core (Antarctica)–Climatic implications, *J. Atmos. Chem.*, *1*, 215–239, 1984.

Delmonte, B., J. R. Petit, and V. Maggi, Glacial to Holocene implications of the new 27,000-year dust record from the EPICA Dome C (East Antarctica) ice core, *Clim. Dyn.*, *18*(8), 647–660, 2002.

Fuchs, N. A., *The Mechanics of Aerosols*, Pergamon, New York, 1964.

Fuhrer, K., E. W. Wolff, and S. J. Johnsen, Timescales for dust variability in the Greenland Ice Core Projct (GRIP) ice core in the last 100,000 years, *J. Geophys. Res.*, *104*(D24), 31,043–31,052, 1999.

Gillette, D. A., I. H. J. Blifford, and D. W. Fryrear, The influence of wind velocity on the size distributions of aerosols generated by the wind erosion of soils, *J. Geophys. Res.*, *79*(D27), 4068–4075, 1974.

Gillette, D. A., J. Adams, A. Endo, and D. Smith, Threshold velocities for input of soil particles into the air by desert soils, *J. Geophys. Res.*, *85*(C10), 5621–5630, 1980.

Grootes, P. M., and M. Stuiver, Oxygen 18/16 variability in Greenland snow and ice with 10-3- to 10-5- year time resolution, *J. Geophys. Res.*, *102*(C12), 26,455–26,470, 1997.

Hansson, M. E., The Renland ice core: A nothern hemisphere record of aerosol composition over 120,000 years, *Tellus, Ser. B*, *46*, 390–418, 1994.

Janecek, T. R., and D. K. Rea, Quaternary fluctuations in the northern hemisphere trade winds and westerlies, *Quat. Res.*, *24*, 150–163, 1985.

Johnsen, S. J., et al., The $\delta^{18}O$ record along the Greenland Ice Core Project deep ice core and the problem of possible Eemian climatic instability, *J. Geophys. Res.*, *102*(C12), 26,397–26,410, 1997.

Junge, C. E., Processes responsible for the trace content in precipitation, in *Isotopes and Impurities in Ice and Snow*, *IAHS-AISH Publ. 118*, Int. Assoc. Hydrol. Sci., Grenoble, 1977.

Kahl, J. D. W., D. A. Martinez, H. Kuhns, C. I. Davidson, J.-L. Jaffrezo, and J. M. Harris, Air mass trajectories to Summit, Greenland: A 44-year climatology and some episodic events, *J. Geophys. Res.*, *102*(C12), 26,861–26,875, 1997.

Kapsner, W. R., R. B. Alley, C. A. Shuman, S. Anandakrishnan, and P. M. Grootes, Dominant influence of atmospheric circulation on snow accumulation in Greenland over the past 18,000 years, *Nature*, *373*, 52–54, 1995.

Krinner, G., and C. Genthon, GCM simulations of the Last Glacial Maximum surface climate of Greenland and Antarctica, *Clim. Dyn.*, *14*, 741–758, 1998.

Lagroix, F., and S. K. Banerjee, Paleowind directions from the magnetic fabric of loess profiles in central Alaska, *Earth Planet. Sci. Lett.*, *195*, 99–112, 2002.

Lamy, F., D. Hebbeln, and G. Wefer, High-resolution marine records of climatic change in mid-latitude Chile during the last 28,000 years based on terrigenous sediment parameters, *Quat. Res.*, *51*, 83–93, 1999.

Mahowald, N., K. Kohfeld, M. Hansson, Y. Balkanski, S. P. Harrison, I. C. Prentice, M. Schulz, and H. Rodhe, Dust sources and deposition during the last glacial maximum and current climate: A comparison of model results with paleodata from ice cores and marine sediments, *J. Geophys. Res.*, *104*(D13), 15,895–15,916, 1999.

Mayewski, P. A., et al., Changes in atmospheric circulation and ocean ice cover over the North Atlantic during the last 41,000 years, *Science*, *263*, 1747–1751, 1994.

Petit, J.-R., M. Briat, and A. Royer, Ice age aerosol content from East Antarctic ice core samples and past wind strength, *Nature*, *293*, 391–394, 1981.

Petit, J. R., L. Mounier, J. Jouzel, Y. S. Korotkevich, V. I. Kotlyakov, and C. Lorius, Palaeoclimatological and chronological implications of the Vostok core dust record, *Nature*, *343*, 56–58, 1990.

Porter, S. C., and A. Zhisheng, Correlation between climate events in the North Atlantic and China during the last glaciation, *Nature*, *375*, 305–308, 1995.

Pye, K., *Aeolian Dust and Dust Deposits*, Academic, San Diego, Calif., 1987.

Rea, D. K., The paleoclimatic record provided by Aeolian deposition in the deep sea: The geologic history of wind, *Rev. Geophys.*, *32*(2), 159–195, 1994.

Röthlisberger, R., M. Bigler, A. Hutterli, S. Sommer, B. Stauffer, H. G. Junghans, and D. Wagenbach, Technique for continious high-resolution analysis of trace substances in firn and ice cores, *Environ. Sci. Technol.*, *34*, 338–342, 2000.

Royer, A., M. De Angelis, and J. R. Petit, A 30,000 year record of physical and optical properties of microparticles from an East Antarctic ice core and implications for paleoclimate reconstruction models, *Clim. Change*, *4*, 381–412, 1983.

Ruth, U., D. Wagenbach, M. Bigler, J. P. Steffensen, and R. Röthlisberger, High resolution dust profiles at NGRIP: Case studies of the calcium-dust relationship, *Ann. Glaciol.*, *35*, in press, 2002.

Saey, P., Concentration and size distribution of microparticles in Alpine and polar ice cores (in German), M.Sc. thesis, Univ. of Heidelberg, Heidelberg, Germany, 1998.

Sehmel, G. A., Particle and gas dry deposition: A review, *Atmos. Environ.*, *14*, 983–1011, 1980.

Steffensen, J. P., Microparticles and chemical impurities in ice cores from Dye 3, South Greenland and their interpretation in palaeoclimatic reconstructions, Ph.D. thesis, Univ. of Copenhagen, Copenhagen, 1995.

Steffensen, J. P., The size distribution of microparticles from selected segments of the Greenland Ice Core Project ice core representing different climatic periods, *J. Geophys. Res.*, *102*(C12), 26,755–26,763, 1997.

Sugimae, A., Elemental constituents of atmospheric particulates and particle density, *Nature*, *307*, 145–147, 1984.

Svensson, A., P. E. Biscaye, and F. E. Grousset, Characterization of late glacial continental dust in the Greenland Ice Core Projct ice core, *J. Geophys. Res.*, *105*(D24), 4637–4656, 2000.

Tegen, I., and I. Fung, Modeling of mineral dust in the atmosphere: Sources, transport, and optical thickness, *J. Geophys. Res.*, *99*(D11), 22,897–22,914, 1994.

Tegen, I., and D. Rind, Influence of the latitudinal temperature gradient on soil dust concentration and deposition in Greenland, *J. Geophys. Res.*, *105*(D6), 7199–7212, 2000.

Thompson, L. G., Variations in microparticle concentration, size distribution, size distribution and elemental composition found in Camp Century, Greenland, and Byrd Station, Antarctica, deep ice cores, in *Isotopes and Impurities in Snow and Ice*, *IAHS-AISH Publ. 118*, pp. 351–363, Int. Assoc. Hydrol. Sci., Grenoble, 1977.

Unnerstad, L., and M. Hansson, Simulated airborne particle size distributions over Greenland during Last Glacial Maximum, *Geophys. Res. Lett.*, *28*(2), 287–290, 2001.

Wagenbach, D., and K. Geis, The mineral dust record in a high altitude Alpine glacier (Colle Gnifetti, Swiss Alps), in *Paleoclimatology and Paleometeorology: Modern and Past Patterns of Global Atmospheric Transprot*, edited by M. Leinen and M. Sarnthein, pp. 543–564, Kluwer Acad., Norwell, Mass., 1989.

Wang, Y. J., H. Cheng, R. L. Edwards, Z. S. An, J. Y. Wu, C.-C. Shen, and J. A. D'Orale, A high-resolution absolute-dated late pleistocene Monsoon record from Hulu cave, China, *Science*, *294*, 2345–2348, 2001.

Werner, M., U. Mikolajewicz, M. Heimann, and G. Hoffmann, Borehole versus isotope temperatures on Greenland: Seasonality does matter, *Geophys. Res. Lett.*, *27*(5), 723–726, 2000.

Wurzler, S., T. G. Reisin, and Z. Levin, Modification of mineral dust particles by cloud processing and subsequent effects on drop size distributions, *J. Geophys. Res.*, *105*(D4), 4501–4512, 2000.

Zdanowicz, C. M., G. A. Zielinski, and C. P. Wake, Characteristics of modern atmospheric dust deposition in snow on the Penny ice cap, Baffin Island, Arctic Canada, *Tellus, Ser. B*, *50*, 506–520, 1998.

Zdanowicz, C. M., G. A. Zielinski, and C. P. Wake, A holocene record of atmospheric dust deposition on the Penny ice cap, Baffin Island, Canada, *Quat. Res.*, *53*, 62–69, 2000.

Zielinski, G. A., Paleoenvironmental implications of the insoluble microparticle record in the GISP2 (Greenland) ice core during the rapidly changing climate of the Pleistocene-Holocene transition, *Geol. Soc. Am. Bull.*, *109*(5), 547–559, 1997.

M. Bigler, Department of Climate and Environmental Physics, University of Bern, CH-3012 Bern, Switzerland.

U. Ruth and D. Wagenbach, Institute of Environmental Physics, University of Heidelberg, 69120 Heidelberg, Germany. (urs.ruth@urz.uni-heidelberg.de)

J. Steffensen, Department of Geophysics, University of Copenhagen, DK-2100 Copenhagen, Denmark.